

Electronic Supplementary Information file

Soft Matter, 2021, DOI: 10.1039/D1SM01242H

Square-triangle tilings : An infinite playground for soft matter

Marianne Impéror-Clerc,^{*a} Anuradha Jagannathan,^a
Pavel Kalugin,^a and Jean-François Sadoc^a

A Lift in 4D

A.1 Geometry in 4D

Here are introduced a few useful geometrical features of the Euclidean space in four dimensions. In a 4D orthonormal basis of four unit vectors, labelled $(\mathbf{I}, \mathbf{J}, \mathbf{K}, \mathbf{L})$, any 4D-vector \mathbf{X} has four coordinates:

$$\mathbf{X} = x\mathbf{I} + y\mathbf{J} + x_{\perp}\mathbf{K} + y_{\perp}\mathbf{L} \quad (31)$$

A 2D-plane of the 4D space is defined by two non-colinear 4D-vectors through the origin. To the orthonormal basis, a set of six 2D-planes can be associated: (\mathbf{I}, \mathbf{J}) , (\mathbf{I}, \mathbf{K}) , (\mathbf{I}, \mathbf{L}) , (\mathbf{J}, \mathbf{K}) , (\mathbf{J}, \mathbf{L}) and (\mathbf{K}, \mathbf{L}) . Among them, two orthogonal 2D-planes, (\mathbf{I}, \mathbf{J}) and (\mathbf{K}, \mathbf{L}) are selected to play a special role, as they are used to represent any 4D-vector \mathbf{X} by its two projections onto them. It is this projection scheme that is used in the lift construction, keeping always the same two 2D-planes. The two sets of coordinates (x, y) and (x_{\perp}, y_{\perp}) can be represented separately onto two Euclidean planes, labelled respectively P and P_{\perp} . The four-dimensional Euclidean space can be defined as the orthogonal direct sum $P \oplus P_{\perp}$ where the planes P and P_{\perp} are two embedded 2D orthogonal subspaces. By extension, the 2D-plane in 4D containing the 4D-vectors of coordinates $(x, y, 0, 0)$ is also named P .

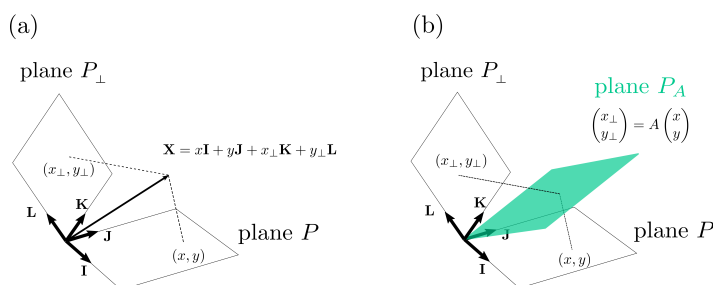


Fig. 18 Geometry in 4D: (a) 4D-vector (b) 2D-plane P_A and its hyperslope (given by a 2×2 matrix A) relative to the plane P .

In general, a 2D-plane P_A can be defined by the linear combination of two non-colinear 4D-vectors of coordinates (a, b, c, d) and (e, f, g, h) in the $(\mathbf{I}, \mathbf{J}, \mathbf{K}, \mathbf{L})$ orthonormal basis. A 4D-vector is in the 2D-plane P_A if it is of the form:

$$\mathbf{X} = \begin{pmatrix} x \\ y \\ x_{\perp} \\ y_{\perp} \end{pmatrix} = \lambda \begin{pmatrix} a \\ b \\ c \\ d \end{pmatrix} + \mu \begin{pmatrix} e \\ f \\ g \\ h \end{pmatrix} \quad (32)$$

where λ and μ are two linear coefficients. This linear relation can be expressed equivalently as follows:

$$\begin{pmatrix} x_{\perp} \\ y_{\perp} \end{pmatrix} = A \begin{pmatrix} x \\ y \end{pmatrix} \quad (33)$$

where A is a (2×2) matrix:

$$A = \begin{pmatrix} A_{x_{\perp}x} & A_{x_{\perp}y} \\ A_{y_{\perp}x} & A_{y_{\perp}y} \end{pmatrix} = \begin{pmatrix} \frac{cf-bg}{af-be} & \frac{ag-ce}{af-be} \\ \frac{df-bh}{af-be} & \frac{ah-de}{af-be} \end{pmatrix} \quad (34)$$

The geometrical interpretation of the matrix A is the hyperslope of the 2D-plane P_A with respect to the plane P and it contains 4 coefficients in the general case. In a symmetric matrix, $A_{x_{\perp}y} = A_{y_{\perp}x}$ and only three independent coefficients are present. Such symmetric matrices are noted B in the main text.

Finally, we introduce a second orthonormal basis, $(\mathbf{I}', \mathbf{J}', \mathbf{K}', \mathbf{L}')$, as it may simplify some relations :

$$\mathbf{I}' = \frac{\mathbf{I} + \mathbf{K}}{\sqrt{2}}, \mathbf{J}' = \frac{\mathbf{I} - \mathbf{K}}{\sqrt{2}}, \mathbf{K}' = \frac{\mathbf{J} + \mathbf{L}}{\sqrt{2}}, \mathbf{L}' = \frac{\mathbf{J} - \mathbf{L}}{\sqrt{2}} \quad (35)$$

A.2 4D lattice for the lift of square-triangle tilings

The standard construction of the lifting of a square-triangle tiling of the Euclidean plane P is detailed here following the literature.^{21,27} Coming back to the six different orientations for edges (see Figure 2), one can observe that only four of six vectors $\mathbf{e}_1, \dots, \mathbf{e}_6 \in P$ given by the formula (1) are linearly independent over \mathbb{Z} (for instance, $\mathbf{e}_5 = \mathbf{e}_3 - \mathbf{e}_1$ and $\mathbf{e}_6 = \mathbf{e}_4 - \mathbf{e}_2$). Therefore, any vertex \mathbf{v} of a square-triangle tiling is naturally indexed by 4 integers n_1, \dots, n_4 :

$$\mathbf{v} = \sum_{i=1}^4 n_i \mathbf{e}_i. \quad (36)$$

as it belongs to the \mathbb{Z} -module of rang 4 spanned by the vectors $\mathbf{e}_1, \dots, \mathbf{e}_4$. One can associate with the vertex \mathbf{v} its counterpart \mathbf{v}_{\perp} in another Euclidean plane P_{\perp} (the so-called “inner” or “perpendicular” space) :

$$\mathbf{v}_{\perp} = \sum_{i=1}^4 n_i \mathbf{e}_{i_{\perp}}, \quad (37)$$

where the vectors $\mathbf{e}_{i_{\perp}}$ have the following coordinates (in some fixed orthonormal basis of P_{\perp}):²¹

$$\mathbf{e}_{i_{\perp}} = a \begin{pmatrix} \cos \frac{7\pi(i-1)}{6} \\ \sin \frac{7\pi(i-1)}{6} \end{pmatrix} \quad (38)$$

The four-dimensional Euclidean space used for the lift construction is defined as the orthogonal direct sum $P \oplus P_{\perp}$. This space contains the planes P and P_{\perp} as orthogonal two-dimensional subspaces. The “lifted” version of any vertex \mathbf{v} is defined as the 4D-vertex $\mathbf{V} = (\mathbf{v}, \mathbf{v}_{\perp}) \in P \oplus P_{\perp}$. Thus, the 4D vertices of the lifted tiling belong to a lattice spanned by four basis vectors $\mathbf{e}_i = (\mathbf{e}_i, \mathbf{e}_{i_{\perp}})$ in $P \oplus P_{\perp}$:

$$\mathbf{V} = (\mathbf{v}, \mathbf{v}_{\perp}) = \sum_{i=1}^4 n_i \mathbf{e}_i = \sum_{i=1}^4 n_i (\mathbf{e}_i, \mathbf{e}_{i_{\perp}}) \quad (39)$$

In this way, the lift of any square-triangle tiling is a subset off the 4D periodic lattice with the basis $\{\mathbf{e}_1, \mathbf{e}_2, \mathbf{e}_3, \mathbf{e}_4\}$. It is worth noting that this 4D lattice is not cubic (for instance, all vectors \mathbf{e}_i have the norm $a\sqrt{2}$ and the volume of the unit cell is $3a^2$). Instead, this lattice can be considered as a direct sum of regular triangular lattices belonging to two orthogonal 2D-planes in the space $P \oplus P_{\perp}$, which we denote by $P_{T_{13}}$ and $P_{T_{24}}$. The 2D-plane

$P_{T_{13}}$ is defined by the two 4D vectors $\boldsymbol{\epsilon}_1$ and $\boldsymbol{\epsilon}_3$, with vertices $(\mathbf{v}, \mathbf{v}_\perp) = n_1 \boldsymbol{\epsilon}_1 + n_3 \boldsymbol{\epsilon}_3$. Similarly, the two lattice vectors $\boldsymbol{\epsilon}_2$ and $\boldsymbol{\epsilon}_4$ define the 2D-plane $P_{T_{24}}$. In Fig. 19, a scheme illustrates these relationships, underlining the fact that the two 2D-planes $P_{T_{13}}$ and $P_{T_{24}}$ are orthogonal to each other, but not to P and P_\perp .

The coordinates of the 4D-vectors $\{\boldsymbol{\epsilon}_1, \boldsymbol{\epsilon}_2, \boldsymbol{\epsilon}_3, \boldsymbol{\epsilon}_4\}$ in the $(\mathbf{I}, \mathbf{J}, \mathbf{K}, \mathbf{L})$ orthonormal basis introduced previously (see A.1) reads:

$$(\boldsymbol{\epsilon}_1, \boldsymbol{\epsilon}_2, \boldsymbol{\epsilon}_3, \boldsymbol{\epsilon}_4) = a \left(\begin{pmatrix} 1 \\ 0 \\ 1 \\ 0 \end{pmatrix}, \begin{pmatrix} \sqrt{3}/2 \\ 1/2 \\ -\sqrt{3}/2 \\ -1/2 \end{pmatrix}, \begin{pmatrix} 1/2 \\ \sqrt{3}/2 \\ 1/2 \\ \sqrt{3}/2 \end{pmatrix}, \begin{pmatrix} 0 \\ 1 \\ 0 \\ -1 \end{pmatrix} \right) \quad (40)$$

As $\boldsymbol{\epsilon}_i = (\mathbf{e}_i, \mathbf{e}_{i\perp})$, the two first coordinates of $\boldsymbol{\epsilon}_i$ in the orthonormal

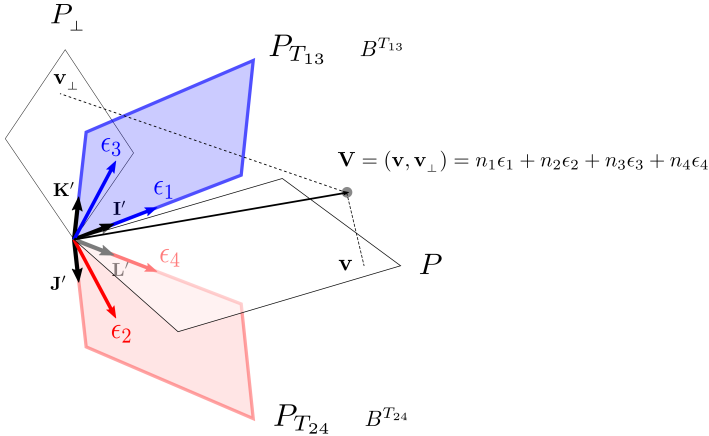


Fig. 19 Scheme of the 4D periodic lattice of basis vectors $\{\boldsymbol{\epsilon}_1, \boldsymbol{\epsilon}_2, \boldsymbol{\epsilon}_3, \boldsymbol{\epsilon}_4\}$.

basis $(\mathbf{I}, \mathbf{J}, \mathbf{K}, \mathbf{L})$ are the coordinates of \mathbf{e}_i in P (see Eq. 1) when the two last ones are the coordinates of $\mathbf{e}_{i\perp}$ in P_\perp (see Eq. 38).

In the second orthonormal basis $(\mathbf{I}', \mathbf{J}', \mathbf{K}', \mathbf{L}')$ introduced in A.1 (see Eq. 35), the basis vectors of the 4D periodic lattice read:

$$\begin{aligned} \boldsymbol{\epsilon}_1 &= a\sqrt{2}\mathbf{I}' \\ \boldsymbol{\epsilon}_2 &= a\sqrt{2}\left(\frac{\sqrt{3}}{2}\mathbf{J}' + \frac{1}{2}\mathbf{L}'\right) \\ \boldsymbol{\epsilon}_3 &= a\sqrt{2}\left(\frac{1}{2}\mathbf{I}' + \frac{\sqrt{3}}{2}\mathbf{K}'\right) \\ \boldsymbol{\epsilon}_4 &= a\sqrt{2}\mathbf{L}' \end{aligned} \quad (41)$$

$$(\boldsymbol{\epsilon}_1, \boldsymbol{\epsilon}_2, \boldsymbol{\epsilon}_3, \boldsymbol{\epsilon}_4)_{\mathbf{I}'\mathbf{J}'\mathbf{K}'\mathbf{L}'} = a\sqrt{2} \left(\begin{pmatrix} 1 \\ 0 \\ 0 \\ 0 \end{pmatrix}, \begin{pmatrix} 0 \\ \sqrt{3}/2 \\ 0 \\ 1/2 \end{pmatrix}, \begin{pmatrix} 1/2 \\ 0 \\ \sqrt{3}/2 \\ 0 \end{pmatrix}, \begin{pmatrix} 0 \\ 0 \\ 0 \\ 1 \end{pmatrix} \right) \quad (42)$$

The fact that the 2D-planes $P_{T_{13}}$ and $P_{T_{24}}$ are orthogonal to each other is obtained here as they identify respectively to $(\mathbf{I}', \mathbf{K}')$ and $(\mathbf{J}', \mathbf{L}')$, two mutually orthogonal 2D-planes generated by basis vectors of the second orthonormal basis. Moreover, in Eq. 42, the direct sum into two triangular lattices is more obvious than in Eq.

40.

A.3 4D reciprocal lattice for diffraction

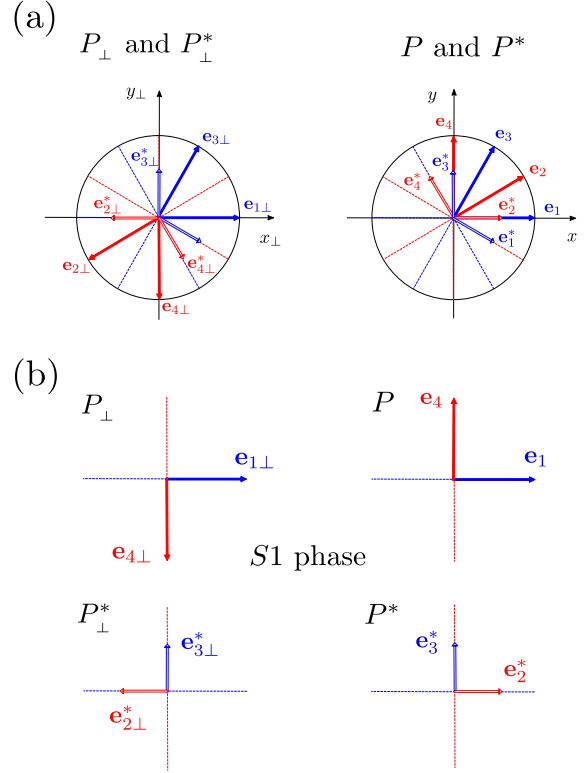


Fig. 20 Reciprocal lattice in 4D. (a) Lattice vectors and associated reciprocal lattice vectors. P^* and P_\perp^* are the reciprocal planes associated to P and P_\perp . (b) Illustration for the pure phase S1 made of square tiles generated by the lattice vectors \mathbf{e}_1 and \mathbf{e}_4 in the plane P .

The 4D reciprocal lattice is defined by generalising the usual definitions in 3D :

$$\boldsymbol{\epsilon}_i \boldsymbol{\epsilon}_j^* = 2\pi \delta_{ij} \quad (43)$$

It leads to the following reciprocal lattice 4D-vectors, expressed in the second orthonormal basis $(\mathbf{I}', \mathbf{J}', \mathbf{K}', \mathbf{L}')$ (see Eq. 35) :

$$\begin{aligned} \boldsymbol{\epsilon}_1^* &= \frac{2\pi}{a\sqrt{2}} \frac{2}{\sqrt{3}} \left(\frac{\sqrt{3}}{2}\mathbf{I}' - \frac{1}{2}\mathbf{K}' \right) \\ \boldsymbol{\epsilon}_2^* &= \frac{2\pi}{a\sqrt{2}} \frac{2}{\sqrt{3}} \mathbf{J}' \\ \boldsymbol{\epsilon}_3^* &= \frac{2\pi}{a\sqrt{2}} \frac{2}{\sqrt{3}} \mathbf{K}' \\ \boldsymbol{\epsilon}_4^* &= \frac{2\pi}{a\sqrt{2}} \frac{2}{\sqrt{3}} \left(-\frac{1}{2}\mathbf{J}' + \frac{\sqrt{3}}{2}\mathbf{L}' \right) \end{aligned} \quad (44)$$

The reciprocal 4D-vectors in the orthonormal basis $(\mathbf{I}, \mathbf{J}, \mathbf{K}, \mathbf{L})$ read:

$$(\mathbf{e}_1^*, \mathbf{e}_2^*, \mathbf{e}_3^*, \mathbf{e}_4^*) = \frac{2\pi}{a\sqrt{3}} \left(\begin{pmatrix} \sqrt{3}/2 \\ -1/2 \\ \sqrt{3}/2 \\ -1/2 \end{pmatrix}, \begin{pmatrix} 1 \\ 0 \\ -1 \\ 0 \end{pmatrix}, \begin{pmatrix} 0 \\ 1 \\ 0 \\ 1 \end{pmatrix}, \begin{pmatrix} -1/2 \\ \sqrt{3}/2 \\ 1/2 \\ -\sqrt{3}/2 \end{pmatrix} \right) \quad (45)$$

The associated 2D lattice vectors in P^* and P_\perp^* are labelled respectively $(\mathbf{e}_1^*, \mathbf{e}_2^*, \mathbf{e}_3^*, \mathbf{e}_4^*)$ and $(\mathbf{e}_{1\perp}^*, \mathbf{e}_{2\perp}^*, \mathbf{e}_{3\perp}^*, \mathbf{e}_{4\perp}^*)$. They are plotted in Figure 20.

B Global uniformity

For the proof of proposition 1 (section 4.2), let us start by proving the “if” statement. Consider an infinite square-triangle tiling with an asymptotically linear lifting map of the form (16) and a sequence of growing patches (\mathcal{P}_i) (see Figure 4) such that the ratio $|\partial\mathcal{P}_i|^2/|\mathcal{P}_i|$ is bounded. Let $J(\mathbf{x})$ stand for the Jacobian derivative of φ :

$$J_{\alpha\beta}(\mathbf{x}) = \frac{\partial\varphi_\alpha(\mathbf{x})}{\partial x^\beta},$$

where the point $\mathbf{x} \in \mathcal{P}_i$ lies in the interior of a tile. This 2×2 matrix-valued function takes five possible values given by the matrices B_Φ from Table 2. Notably, $\det(J(\mathbf{x}))$ equals 1 if \mathbf{x} is inside a triangle and -1 for \mathbf{x} lying inside a square. Therefore, the area-weighted average of $\det(J(\mathbf{x}))$ over \mathcal{P}_i is given by the formula

$$\langle \det(J(\mathbf{x})) \rangle_{\mathcal{P}_i} = |\mathcal{P}_i|^{-1} \int_{\mathcal{P}_i} \det(J(\mathbf{x})) \, d\mathbf{x} = \tau(\mathcal{P}_i) - \sigma(\mathcal{P}_i). \quad (46)$$

By Stokes’ theorem, one can express the integral over the patch \mathcal{P}_i in (46) via an integral over its boundary $\partial\mathcal{P}_i$:

$$\int_{\mathcal{P}_i} \det(J(\mathbf{x})) \, d\mathbf{x} = \int_{\mathcal{P}_i} d\varphi(\mathbf{x}) \wedge d\varphi(\mathbf{x}) = \frac{1}{2} \varepsilon^{\alpha\beta} \oint_{\partial\mathcal{P}_i} \varphi_\alpha(\mathbf{x}) d\varphi_\beta(\mathbf{x}), \quad (47)$$

where $\varepsilon^{\alpha\beta}$ is the Levi-Civita symbol and the integration over $\partial\mathcal{P}_i$ is performed counterclockwise. Since one can always choose the origin of the coordinate system within the patch \mathcal{P}_i , we can safely assume that $\|\mathbf{x}\| < |\partial\mathcal{P}_i|$ for all points in the path of the integral in (47). Then, equation (16) gives rise to the following asymptotic formula:

$$\oint_{\partial\mathcal{P}_i} \varphi_\alpha(\mathbf{x}) d\varphi_\beta(\mathbf{x}) = B_{\alpha\gamma} \oint_{\partial\mathcal{P}_i} x^\gamma d\varphi_\beta(\mathbf{x}) + o(|\partial\mathcal{P}_i|^2). \quad (48)$$

The asymptotic behavior of the integral in (48) can be obtained in the same way:

$$\oint_{\partial\mathcal{P}_i} x^\gamma d\varphi_\beta(\mathbf{x}) = - \oint_{\partial\mathcal{P}_i} \varphi_\beta(\mathbf{x}) dx^\gamma = -B_{\beta\delta} \oint_{\partial\mathcal{P}_i} x^\delta dx^\gamma + o(|\partial\mathcal{P}_i|^2). \quad (49)$$

By combining equations (46), (47), (48) and (49), and taking into account the following identities:

$$\begin{aligned} \oint_{\partial\mathcal{P}_i} x^\delta dx^\gamma &= \varepsilon^{\delta\gamma} |\mathcal{P}_i| \\ -\frac{1}{2} \varepsilon^{\alpha\beta} \varepsilon^{\delta\gamma} B_{\alpha\gamma} B_{\beta\delta} &= \det(B), \end{aligned}$$

we obtain

$$\tau(\mathcal{P}_i) - \sigma(\mathcal{P}_i) = \det(B) + o\left(\frac{|\partial\mathcal{P}_i|^2}{|\mathcal{P}_i|}\right). \quad (50)$$

Consider now the area-weighted average of $J(\mathbf{x})$ over the patch \mathcal{P}_i :

$$\langle J_{\alpha\beta} \rangle_{\mathcal{P}_i} = \frac{1}{|\mathcal{P}_i|} \int_{\mathcal{P}_i} J_{\alpha\beta}(\mathbf{x}) \, d^2\mathbf{x}. \quad (51)$$

Again, using Stokes’ theorem we get

$$\langle J_{\alpha\beta} \rangle_{\mathcal{P}_i} = \frac{\varepsilon^{\beta\gamma}}{2|\mathcal{P}_i|} \oint_{\partial\mathcal{P}_i} \varphi_\alpha(\mathbf{x}) dx^\gamma$$

As follows from equation (16), the above integral behaves asymptotically as

$$\oint_{\partial\mathcal{P}_i} \varphi_\alpha(\mathbf{x}) dx^\gamma = B_{\alpha\delta} \oint_{\partial\mathcal{P}_i} x^\delta dx^\gamma + o(|\partial\mathcal{P}_i|^2) = B_{\alpha\delta} \varepsilon^{\delta\gamma} |\mathcal{P}_i| + o(|\partial\mathcal{P}_i|^2).$$

This gives rise to the following estimate of $\langle J \rangle_{\mathcal{P}_i}$:

$$\langle J_{\alpha\beta} \rangle_{\mathcal{P}_i} = B_{\alpha\beta} + o\left(\frac{|\partial\mathcal{P}_i|^2}{|\mathcal{P}_i|}\right). \quad (52)$$

The integral in (51) can also be computed as a sum of contributions of individual tile species, yielding

$$\begin{aligned} \langle J \rangle_{\mathcal{P}_i} &= \sigma_1(\mathcal{P}_i) B^{S1} + \sigma_2(\mathcal{P}_i) B^{S2} + \sigma_3(\mathcal{P}_i) B^{S3} + \\ &\quad + \tau_{13}(\mathcal{P}_i) B^{T13} + \tau_{24}(\mathcal{P}_i) B^{T24}, \end{aligned} \quad (53)$$

where the matrices B^{S1} , B^{S2} , B^{S3} , B^{T13} and B^{T24} are given in Table 2. Since these matrices are symmetric, this equation contains three linear constraints on the area fractions of different tile species in \mathcal{P}_i . Together with (46) and the condition

$$\sigma_1(\mathcal{P}_i) + \sigma_2(\mathcal{P}_i) + \sigma_3(\mathcal{P}_i) + \tau_{13}(\mathcal{P}_i) + \tau_{24}(\mathcal{P}_i) = 1$$

these constraints fix entirely the area fractions in terms of $\langle J_{\alpha\beta} \rangle_{\mathcal{P}_i}$ and $\langle \det(J(\mathbf{x})) \rangle_{\mathcal{P}_i}$. On the other hand, since $|\partial\mathcal{P}_i|^2/|\mathcal{P}_i|$ is assumed bounded, equations (52) and (50) read as

$$\lim_{i \rightarrow \infty} \langle J_{\alpha\beta} \rangle_{\mathcal{P}_i} = B_{\alpha\beta}$$

and

$$\lim_{i \rightarrow \infty} \langle \det(J(\mathbf{x})) \rangle_{\mathcal{P}_i} = \det(B).$$

Therefore, the area fractions $\sigma_1(\mathcal{P}_i)$, $\sigma_2(\mathcal{P}_i)$, $\sigma_3(\mathcal{P}_i)$, $\tau_{13}(\mathcal{P}_i)$ and $\tau_{24}(\mathcal{P}_i)$ have well-defined limits (see eq. (3)) and the considered tiling is globally uniform.

Let us now prove the “only if” part of Proposition 1. We shall proceed by *reductio ad absurdum*. Let us assume that there exists a globally uniform tiling such that its lifting map φ is not asymptotically linear. For a globally uniform tiling one can define the matrix B by the formula

$$B_{\alpha\beta} = \lim_{|\mathcal{P}_i| \rightarrow \infty} \langle J_{\alpha\beta} \rangle_{\mathcal{P}_i}, \quad (54)$$

for any sequence of patches \mathcal{P}_i , such that the ratio $|\partial\mathcal{P}_i|^2/|\mathcal{P}_i|$ is bounded. By the hypothesis, there should exist a real constant $M > 0$ such that one can a vector $\mathbf{x} \in P$ of an arbitrarily large norm $l = \|\mathbf{x}\|$ for which

$$\|\varphi(\mathbf{x}) - B \cdot \mathbf{x}\| > Ml. \quad (55)$$

Let us consider a rectangle $\mathcal{R} \subset P$ of dimensions $l \times \frac{Ml}{2}$ such that

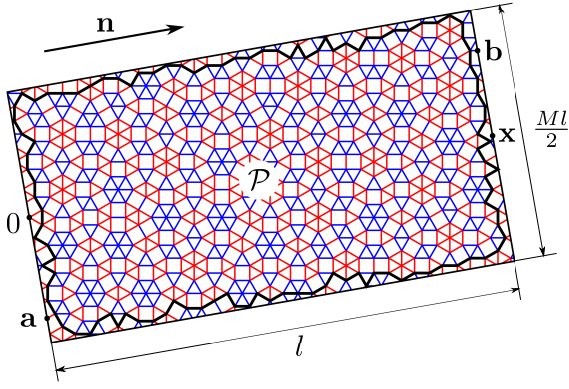


Fig. 21 The rectangular region \mathcal{R} used in the proof of Proposition 1. The bold broken line is the boundary of the largest tiling patch \mathcal{P} contained within \mathcal{R} .

the points 0 and \mathbf{x} are the centers of its edges of length $\frac{Ml}{2}$ (see Figure 21). Denote by n^β the components of the unit vector $\mathbf{n} = \mathbf{x}/\|\mathbf{x}\|$. By Stoke's theorem, we get

$$n^\beta \left(\langle J_{\alpha\beta} \rangle_{\mathcal{R}} - B_{\alpha\beta} \right) = \frac{n^\beta \varepsilon_{\beta\gamma}}{Ml^2} \oint_{\partial\mathcal{R}} \left(\varphi_\alpha(\mathbf{x}) - B_{\alpha\delta} x^\delta \right) dx^\gamma \quad (56)$$

The contribution of the edges of \mathcal{R} parallel to \mathbf{x} to the right-hand side of (56) vanishes after multiplication by $n^\beta \varepsilon_{\beta\gamma}$. To estimate the contribution of the remaining two edges, we observe that the integrand in (56) is Lipschitz continuous with Lipschitz constant 2. Indeed, the spectral radius of the Jacobian derivative J (and hence also that of the matrix B in (54)) is bounded by 1. Therefore, taking into account (55), for any two points \mathbf{a} and \mathbf{b} belonging respectively to the edges of \mathcal{R} containing 0 and \mathbf{x} (see Figure 21), one has

$$\begin{aligned} \|\varphi(\mathbf{a}) - B \cdot \mathbf{a}\| &\leq 2\|\mathbf{a}\| \\ \|\varphi(\mathbf{b}) - B \cdot \mathbf{b}\| &\geq Ml - 2\|\mathbf{b} - \mathbf{x}\| \end{aligned} \quad (57)$$

Formulas (57) provide a lower bound for the integral in (56), giving rise to the following inequality

$$\|(\langle J \rangle_{\mathcal{R}} - B) \cdot \mathbf{n}\| \geq \frac{M}{4}.$$

Let now \mathcal{P} stand for the largest patch of the tiling contained within the rectangle \mathcal{R} . As the aspect ratio of \mathcal{R} is fixed, $|\partial\mathcal{P}|^2/|\mathcal{P}|$ is bounded from above by some constant not depending on l . For large l , the contribution of the interstice between \mathcal{P} and \mathcal{R} to $\langle J \rangle_{\mathcal{P}}$ is negligible and one has

$$\|(\langle J \rangle_{\mathcal{P}} - B) \cdot \mathbf{n}\| \geq \frac{M}{4} + o(1) \quad \text{as } l \rightarrow \infty. \quad (58)$$

Since by the assumption the norm of \mathbf{x} can be arbitrarily large, we can construct a sequence of patches \mathcal{P}_i , such that the ratio $|\partial\mathcal{P}_i|^2/|\mathcal{P}_i|$ is bounded from above, but $\|(\langle J \rangle_{\mathcal{P}_i} - B)\|$ is bounded from below, in contradiction with (54). This contradiction proves the statement.

As now the equivalence between the global uniformity and the asymptotic linearity of the lifting map is established, to finish the

proof it remains only to observe that (53) in the limit of infinite tilings gives

$$B = \sigma_1 B^{S1} + \sigma_2 B^{S2} + \sigma_3 B^{S3} + \tau_{13} B^{T13} + \tau_{24} B^{T24}. \quad (59)$$

yielding (17). Similarly, the equation (18) arises as the limit of (46).

C Special phases

C.1 The Σ phase

C.1.1 Structure factor of the Σ phase

The 3^2_{434} vertices have four different orientations depicted in black, blue, magenta and green in the different figures. The edge's size of the centered square unit cell is $a_\Sigma = a(1 + \sqrt{3})$ where a is the edge's size of the tiles. It contains eight vertices when the square primitive unit cell contains four vertices. As pictured in Figure 9, each set of vertices having the same color forms a regular square lattice of edge's size $a(1 + \sqrt{3})/\sqrt{2}$, turned by an angle of $\pi/4$ with respect to the centered square unit cell. Starting from one of these four regular square lattices, the three other ones can be obtained by translation using the three translation vectors \mathbf{e}_1 , \mathbf{e}_3 and $\mathbf{e}_1 - \mathbf{e}_3$.

The 2D structure factor of the Σ phase is defined as the Fourier

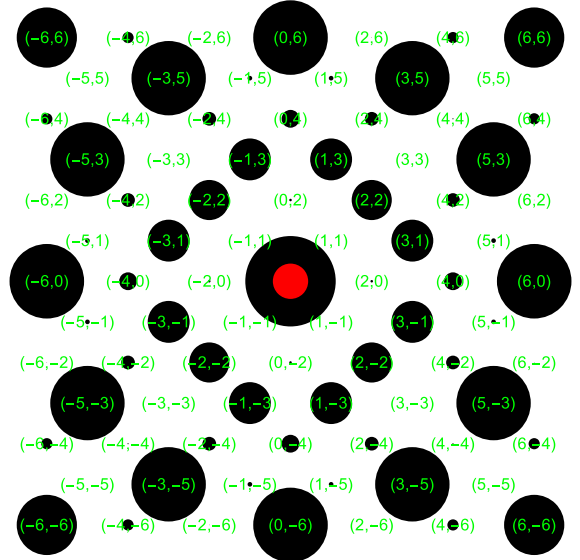


Fig. 22 Detail of the structure factor of the Σ phase including HK indices (see also Figure 10). The twelvefold symmetry is only approximate. The (60) and (53) peaks are not exactly positioned on the same circle ($G_{53}^*/G_{60}^* = 0.9718$) and their intensities are not exactly the same ($I_{53}/I_{60} = 0.9976$).

transform of the points lattice located on the vertices. It can be calculated taking for example the following coordinates of the four vertices in the plane P (using unit vectors $\frac{1}{a}\mathbf{e}_1$ and $\frac{1}{a}\mathbf{e}_4$):

$$(a/2, 0) \quad (-a/2, 0) \quad \left(0, a\sqrt{3}/2\right) \quad \left(0, -a\sqrt{3}/2\right)$$

The 2D structure factor consists in a periodic lattice of diffraction peaks that can be indexed using two integer indices HK

$$\mathbf{G}^*_{HK} = \frac{2\pi}{a\Sigma} \left(H\frac{1}{a}\mathbf{e}_1 + K\frac{1}{a}\mathbf{e}_4 \right) = \frac{2\pi}{a(1+\sqrt{3})} \left(H\frac{1}{a}\mathbf{e}_1 + K\frac{1}{a}\mathbf{e}_4 \right) \quad (60)$$

and the intensities of the Bragg peaks are $I_{HK} = |F_{HK}|^2$ with:

$$F_{HK} = 2 \left[1 + (-1)^{(H+K)} \right] \left[\cos \left(\frac{\pi}{1+\sqrt{3}} H \right) + \cos \left(\frac{\pi\sqrt{3}}{1+\sqrt{3}} K \right) \right] \quad (61)$$

The 2D structure factor is shown in Figures 10 and 22. A remarkable feature is that the modulations in the intensities are not periodic, as can be seen in the expression of F_{HK} in the cosine terms due to the presence of irrational terms. This is due to the irrational coordinates of the lattice points in the square unit cell. This feature of the structure factor is linked to the intrinsic incommensurability of square-triangle tilings.

In Figure 22, the HK indices are reported for some Bragg peaks. The set of twelve diffraction peaks with $(6,0)$ and $(5,3)$ indices is remarkable as it form an approximate figure with 12-fold symmetry. But it is only approximate as the peaks are not exactly positioned all on the same circle ($G_{53}^*/G_{60}^* = 0.9718$) and their intensities are not exactly the same ($I_{53}/I_{60} = 0.9976$), with tiny differences of less than 1 percent.

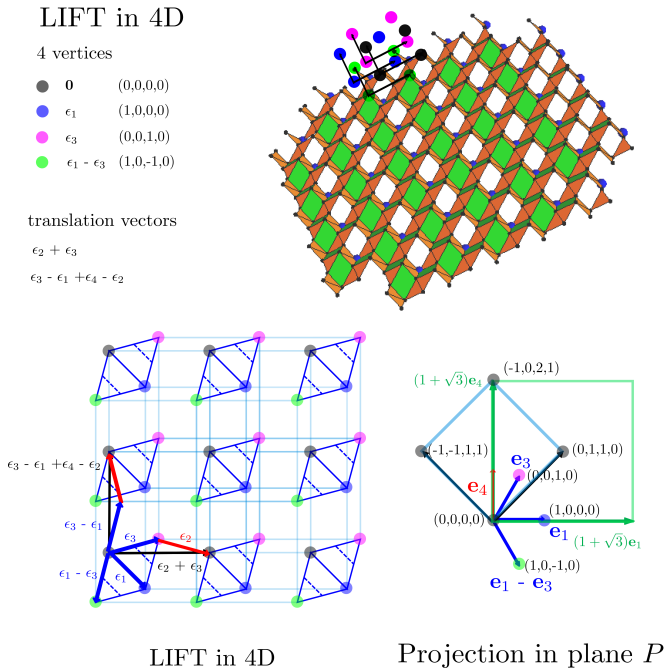


Fig. 23 Lift in 4D of the Σ phase. The 4D vertices are located in four different 2D-planes having the same hyperslope B^Σ and which are translated from each other. In each 2D-plane, the vertices have the same orientation (same color) and form a regular square lattice.

C.1.2 4D lift of the Σ phase

The lift construction in the 4D space consists in associating to each vertex in the plane P a 4D lifted vertex. This association can be done in different ways. Here we choose to place the origin

of the plane P on a black vertex which is lifted to the origin of the 4D space (see Figure 23). A blue vertex near to the origin is lifted to the 4D vertex \mathbf{e}_1 , a magenta one to \mathbf{e}_3 and a green one to $\mathbf{e}_1 - \mathbf{e}_3$. In 4D, all other vertices are obtained by translation. All vertices of the same color are lifted in the same 2D-plane using the two translation vectors $\mathbf{e}_2 + \mathbf{e}_3$ and $\mathbf{e}_3 - \mathbf{e}_1 + \mathbf{e}_4 - \mathbf{e}_2$. The black vertices are embedded in a plane containing the origin when the three other planes are parallel to this plane and can be deduced by translation from the origin using \mathbf{e}_1 (blue vertices), \mathbf{e}_3 (magenta vertices) and $\mathbf{e}_1 - \mathbf{e}_3$ (green vertices).

The expression of the matrix B^Σ is given in Eq. 20. Its expression can be identified to the hyperslope with respect to the plane P (2x2 matrix A , see Eq. 34) of the plane defined by the two vectors $\mathbf{e}_2 + \mathbf{e}_3$ and $\mathbf{e}_3 - \mathbf{e}_1 + \mathbf{e}_4 - \mathbf{e}_2$. It can be verified from the expression of the $(\mathbf{e}_1, \mathbf{e}_2, \mathbf{e}_3, \mathbf{e}_4)$ 4D-vectors in the $(\mathbf{I}, \mathbf{J}, \mathbf{K}, \mathbf{L})$ orthonormal basis (see Eq. 40), leading to:

$$\mathbf{e}_2 + \mathbf{e}_3 = a \begin{pmatrix} \alpha \\ \alpha \\ -\beta \\ \beta \end{pmatrix}; \mathbf{e}_3 - \mathbf{e}_1 + \mathbf{e}_4 - \mathbf{e}_2 = a \begin{pmatrix} -\alpha \\ \alpha \\ \beta \\ \beta \end{pmatrix} \quad (62)$$

with

$$\alpha = (\sqrt{3} + 1)/2; \beta = (\sqrt{3} - 1)/2 \quad (63)$$

Using the general expression of the hyperslope (2x2 matrix A) with respect to the plane P (see Eq. 34), the identity $A = B^\Sigma$ is verified.

To construct the projections in the planes P and P_\perp (see Figure 9), we use the four integer indices notation already introduced in equation 39. The lift construction allows to index each vertex with a unique set of four integers (n_1, n_2, n_3, n_4) writing that $(\mathbf{v}, \mathbf{v}_\perp) = n_1\mathbf{e}_1 + n_2\mathbf{e}_2 + n_3\mathbf{e}_3 + n_4\mathbf{e}_4$. For example, the black 4D vertices have the following 4D integer coordinates where n, m are two integers:

$$(\mathbf{v}, \mathbf{v}_\perp)_{\text{black}} = n(\mathbf{e}_2 + \mathbf{e}_3) + m(\mathbf{e}_3 - \mathbf{e}_1 + \mathbf{e}_4 - \mathbf{e}_2) = \begin{pmatrix} -m \\ n-m \\ n+m \\ m \end{pmatrix} \quad (64)$$

C.1.3 Infinite sequence of phases with the same composition.

To illustrate the fact that, except for the five pure phases, any composition point corresponds to an infinite number of phases, let's consider the following transformation (Figure 24).

It consists in replacing each triangle and square by four identical tiles and applying afterwards a scale factor of two to keep the tile's dimension. This transformation preserves both the ratio N_t/N_s and the tiles orientation distribution so the 3D composition point is fixed. By applying it several times, one can generate an infinite sequence of other phases located at the same composition point. Applied at a composition point like Σ_1 , starting from the Σ phase, an infinite sequence of periodic phases with increasing unit cell size is obtained. Note that all these periodic phases are globally uniform and couldn't be generated by a cut-and-project method. The infinite limit is a coexistence of domains of four pure

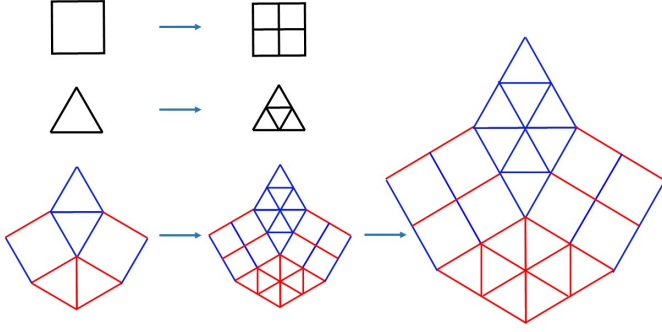


Fig. 24 A simple transformation of tiles generating an infinite sequence of phases at a fixed composition point. The ratio N_i/N_s is preserved as both tiles number are multiplied by a factor four and the tiles orientation distribution is the same as well. It is illustrated at the composition point Σ_1 .

phases around a junction point (see section 6.2).

C.2 Structure factor of the H phase

The 2D structure factor of the Archimedean H phase is calculated in a similar way as for the Σ phase using a rectangular centered lattice of dimensions a and $(2 + \sqrt{3})a$ with two vertices per node at positions $(0, a/2)$ and $(0, -a/2)$ (see Figure 8 for the orientation of the H phase). The 2D structure factor is shown in Figure 25 and consists in a periodic set of Bragg peaks that can be indexed by two integer indices HK of intensities $I_{HK} = |F_{HK}|^2$ with:

$$F_{HK} = 2 \left[1 + (-1)^{(H+K)} \right] \cos \left(\frac{\pi K}{2 + \sqrt{3}} \right) \quad (65)$$

A remarkable feature is the way how the intensities of the

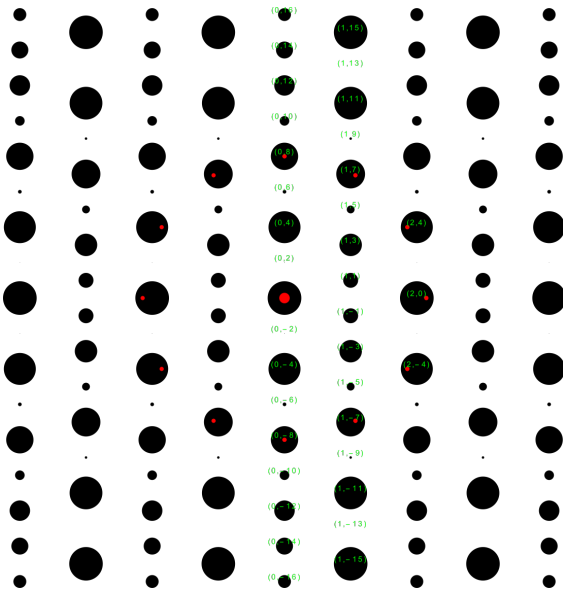


Fig. 25 Structure factor of the H phase. The infinite 1D stripes are horizontal and the stack direction is vertical like in Figure 8.

Bragg peaks are modulated. The whole structure factor can be decomposed in two types of infinite vertical lines of Bragg peaks of intensities I_{0K} with K even and I_{1K} with K odd. Along the horizontal direction, these lines of Bragg peaks alternate in a simple periodic fashion. This is expected because the infinite stripes of tiles along the horizontal direction are periodic (rows of square or triangles) (see Figure 8). But along the vertical direction, the intensities are modulated via the cosine term in eq. 65. Because of the presence of the irrational ratio $2 + \sqrt{3}$, it is impossible for two diffraction peaks to have exactly the same intensity. In other words, even if the cosine function is periodic, it is sampled at irrational values. It comes from the fact the period of the 1D stack of stripes, here $(2 + \sqrt{3})a$, is incommensurate with a .

This aperiodicity in the Bragg peak intensities along the stack direction is a strong signature of the incommensurability between the two tiles dimensions, a and $a\sqrt{3}/2$. In a system where the two tiles dimensions would be in a rational ratio, in the cosine term, this ratio would appear as a fraction of two integers, and the Bragg peaks intensities would exhibit periodic modulations along the stack direction.

One can also notice in Figure 25 that a set of twelve diffraction peaks show an approximate 12-fold symmetry, but this feature is much less striking than for the Σ phase (see Figures 10 and 22). It makes sense as the 3D composition point of the H phase is very asymmetric.

C.3 Striped phases

C.3.1 Stacking sequence and average slope

The stacking sequence is built using two vectors, \mathbf{e}_4 for square tiles and \mathbf{e}_3 for the triangular tiles. The vertices in plane P have the form $\mathbf{v} = n_1 \mathbf{e}_1 + n_3 \mathbf{e}_3 + n_4 \mathbf{e}_4$, with the stripes direction along \mathbf{e}_1 . The stack of the stripes is given by a sequence of vectors \mathbf{e}_3 (stripe of triangular tiles) and \mathbf{e}_4 (stripe of square tiles) that follows a straight line which slope $b(\tau)$ is related to the composition, as illustrated in Figure 11a. Simultaneously in P_\perp , the associated vertices are $\mathbf{v}_\perp = n_1 \mathbf{e}_{1\perp} + n_3 \mathbf{e}_{3\perp} + n_4 \mathbf{e}_{4\perp}$. As a result, in the plane P , the stacking sequence (\mathbf{e}_3 and \mathbf{e}_4 lattice vectors) follows a straight line of slope $b(\tau)$. Similarly, in the plane P_\perp , the stacking sequence (made of $\mathbf{e}_{3\perp}$ and $\mathbf{e}_{4\perp}$ lattice vectors) follows a straight line of slope $b_\perp(\tau)$. The expression of these two slopes read:

$$b(\tau) = \frac{y}{x} = \frac{\sqrt{3}}{\tau}, \quad (66)$$

$$b_\perp(\tau) = \frac{y_\perp}{x_\perp} = \sqrt{3} \frac{\tau - \sigma}{\tau} = \sqrt{3} \frac{2\tau - 1}{\tau}$$

If only square tiles are present ($\tau = 0$), the average slope in the plane P is vertical and the striped phase is the \mathbf{S}_1 pure phase (see Figure 11a). Similarly, for $\tau = 1$, the slope coefficient is equal to $\sqrt{3}$ and the striped phase is the \mathbf{T}_{13} pure phase. For all other compositions, the average slope is in between these two values. In particular, for $\tau = \frac{1}{2}$, $b = 2\sqrt{3}$ (plane P) and $b_\perp = 0$ (plane P_\perp).

This last feature is characteristic of aperiodic order: the stacking sequence in the plane P_{\perp} follows the horizontal line along x_{\perp} .

C.3.2 Staircase

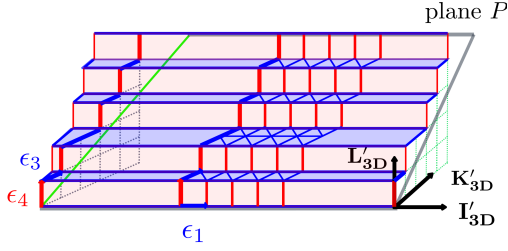


Fig. 26 Lift construction for striped phases. A stacking sequence can be visualized as a '3D staircase'. Each 'step' of the 3D staircase has a vertical side of height $a\sqrt{2}$ and an horizontal side of width $a\sqrt{2}\frac{\sqrt{3}}{2}$. Vertical portions (in red) correspond to the S_1 pure phase when horizontal ones (in blue) correspond to the T_{13} pure phase. The plane defined by the two vectors $(\boldsymbol{\epsilon}_3, \boldsymbol{\epsilon}_4)$ forms a square lattice of parameter $a\sqrt{2}$ and its intersection with the plane P is a line depicted in light green color.

For striped phases, the lift construction in the 4D space is made using only three vectors $(\boldsymbol{\epsilon}_1, \boldsymbol{\epsilon}_3, \boldsymbol{\epsilon}_4)$ instead of 4 in the general case. The stacking sequence is expressed onto the two 4D lattice vectors $\boldsymbol{\epsilon}_3$ and $\boldsymbol{\epsilon}_4$. The lifted version of a striped phase can be visualised as a "staircase" (Figure 26). To do so, one can define a 3D subspace of the 4D space by taking all components along \mathbf{J}' equal to zero. In this 3D subspace, all vectors have three components in an orthonormal basis $(\mathbf{I}'_{3D}, \mathbf{K}'_{3D}, \mathbf{L}'_{3D})$ which is derived from the second 4D orthonormal basis (Eq. 42) and the lattice vectors read:

$$\begin{aligned} \boldsymbol{\epsilon}_{1,3D} &= a\sqrt{2}\mathbf{I}'_{3D} \\ \boldsymbol{\epsilon}_{3,3D} &= a\sqrt{2}\left(\frac{1}{2}\mathbf{I}'_{3D} + \frac{\sqrt{3}}{2}\mathbf{K}'_{3D}\right) \\ \boldsymbol{\epsilon}_{4,3D} &= a\sqrt{2}\mathbf{L}'_{3D} \end{aligned}$$

$$(\boldsymbol{\epsilon}_{1,3D}, \boldsymbol{\epsilon}_{3,3D}, \boldsymbol{\epsilon}_{4,3D})_{\mathbf{I}'_{3D}, \mathbf{K}'_{3D}, \mathbf{L}'_{3D}} = a\sqrt{2} \left(\begin{pmatrix} 1 \\ 0 \\ 0 \end{pmatrix}, \begin{pmatrix} 1/2 \\ \sqrt{3}/2 \\ 0 \end{pmatrix}, \begin{pmatrix} 0 \\ 0 \\ 1 \end{pmatrix} \right) \quad (67)$$

The steps of the '3D-staircase' (see Figure 26) are along \mathbf{L}'_{3D} (with a vertical edge of height $a\sqrt{2}$) and along \mathbf{K}'_{3D} with a width $a\sqrt{2}\frac{\sqrt{3}}{2}$, corresponding to the coordinate of $\boldsymbol{\epsilon}_{3,3D}$ along \mathbf{K}'_{3D} . Embedded in this 3D subspace, the plane P is constructed with the two vectors basis $(\mathbf{I}'_{3D}, \mathbf{K}'_{3D} + \mathbf{L}'_{3D})$ and the plane P_{\perp} with $(\mathbf{I}'_{3D}, \mathbf{K}'_{3D} - \mathbf{L}'_{3D})$. P and P_{\perp} are still orthogonal to each other and are turned by an angle of $\pi/4$ along \mathbf{I}'_{3D} . The intersection between the plane P and the plane $(\boldsymbol{\epsilon}_{3,3D}, \boldsymbol{\epsilon}_{4,3D})$ is along the direction $(1, \sqrt{3}, \sqrt{3})$. The irrational slope $\frac{\sqrt{3}}{2}$ (see Eq. 22) is obtained writing that this direction is along the 3D-vector $2(\frac{1}{2}\mathbf{I}'_{3D} + \frac{\sqrt{3}}{2}\mathbf{K}'_{3D}) + \sqrt{3}\mathbf{L}'_{3D}$. The plane defined by the two vectors

$(\boldsymbol{\epsilon}_{3,3D}, \boldsymbol{\epsilon}_{4,3D})$ form a square lattice of parameter $a\sqrt{2}$. Note that this plane is tilted by an angle of $\pi/3$ along the vertical direction \mathbf{L}'_{3D} , where $(\mathbf{I}'_{3D}, \mathbf{K}'_{3D}, \mathbf{L}'_{3D})$ is a 3D orthonormal basis. The plane P is inclined at an angle of $\pi/4$ along the direction $\mathbf{K}'_{3D} + \mathbf{L}'_{3D}$. The intersection of the plane P with the plane $(\boldsymbol{\epsilon}_{3,3D}, \boldsymbol{\epsilon}_{4,3D})$ is a line shown with a light green color.

D Inflation constructions

D.1 Striped phases: 1D aperiodic order

Starting from some initial "seed", a longer sequence is constructed by using the following substitution rules: 1) each stripe s is replaced by a copies of s and four stripes t and 2) each stripe t is replaced by 3 stripes s and a copies of t , where $a \geq 0$ is an integer. Upon iteration, these substitution rules generate periodic phases with bigger and bigger unit cell, and one approaches a perfect 1D quasiperiodic structure at the limit of an infinite number of iterations. An example of the first three steps of a construction corresponding to $a = 3$ is shown in Fig. 12b.

If the number of s strips, $N_s^{(i)}$, and the number of t strips $N_t^{(i)}$ at the i th step are known, their number at the $i + 1$ th step can be readily found, since the substitution rules imply that

$$\mu_{i+1} = \begin{pmatrix} a & 4 \\ 3 & a \end{pmatrix} \mu_i \quad (68)$$

where $\mu_i = \{N_s^{(i)}, N_t^{(i)}\}$.³² The maximal eigenvalue (called the Perron root) of the 2 by 2 matrix of this equation and its corresponding eigenvector provide information on, respectively, the rate of growth of the tiling, and on the relative proportion of s and t type strips. This eigenvalue is $(a + 2\sqrt{3})$, for all values of the integer parameter a , and the corresponding eigenvector is $\{\sqrt{3}/2, 1\}$. This shows that the ratio of triangles to squares tends towards the value $\sqrt{3}/2$.

D.2 Maximally symmetric phases

The initial seed is a dodecagonal wheel (see Figure 13). Its composition is maximally symmetric. It contains the same number of T1/T3 (blue color) and T2/T4 (red color) triangles ($N_{t,12,0} = N_{t,34,0} = 6$), and the same number for each of the three kinds of squares ($N_{s,1,0} = N_{s,2,0} = N_{s,3,0} = 2$). For the seed, the ratio $N_{t,0}/N_{s,0} = 12/6 = 2$ has a rational value. After an infinite number of iterations tends, this ratio in tiles number reaches the irrational value $N_t/N_s = 4/\sqrt{3}$.

Initial conditions are $N_{t,0} = 12$ and $N_{s,0} = 6$. If we denote by $N_{t,i}$ and $N_{s,i}$ the number of triangles and squares at inflation step i , after the next inflation step, these numbers are given by $N_{t,i+1} = 7N_{t,i} + 3N_{s,i}$ and $N_{s,i+1} = 16N_{t,i} + 7N_{s,i}$. This is encoded in the following transfer matrix form to compute the vector $\mathbf{v}_i = \{N_{t,i}, N_{s,i}\}$:

$$\mathbf{v}_{i+1} = \begin{pmatrix} 7 & 3 \\ 16 & 7 \end{pmatrix} \mathbf{v}_i \quad (69)$$

To the Perron root $(7 + 4\sqrt{3})$ of this matrix corresponds an eigenvector $\{\sqrt{3}/4, 1\}$. It is easily checked that the limiting value of the ratio of tiles is $N_t/N_s = 4/\sqrt{3}$.

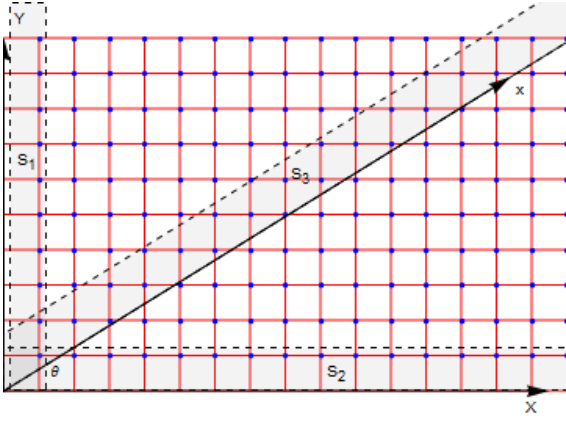


Fig. 27 Selection stripes for i) the periodic sequence of B-tiles (S_1 , $\theta = \pi/2$) ii) the periodic sequence of A-tiles (S_2 , $\theta = 0$) and iii) the Fibonacci quasiperiodic sequence (S_3 , $\theta = \arctan(1/\lambda_1)$). Selected points are projected onto the "physical" x axis, giving rise to a sequence of A and B tiles.

To obtain the dodecagonal QC phase shown in Fig. 13a, the following rule is followed.³² If there are a majority of blue bonds emanating from the 'parent' site then the dodecagon contains a B hexagon, and otherwise it contains the R hexagon. Note that in this construction, it is impossible to get four squares around a site during the inflation process, so the rule can always be applied, in the interior of the patch. For the sites located on the border of the patch at a given iteration step, one needs to examine the environment of that after the next iteration step. This is the rule applied to obtain the patch after one inflation step.

E Diffraction

In this section we discuss some properties of the structure factor, $S(\vec{q})$, a physical quantity which is measurable by a diffraction experiment and useful to distinguish between different types of spatial organization of particles. It is defined by $VS(\vec{q}) = |\rho(\vec{q})|^2$ where V is the volume of the sample and $\rho(\vec{q})$ is the Fourier transform of the spatial density. We will consider the simplest situation in which unit point masses are located at each vertex, $\rho(\vec{r}) = \sum_j \delta(\vec{r} - \vec{R}_j)$ where $\delta(\vec{r})$ is a delta-function and \vec{R}_j are the positions of the N particles $j = 1, \dots, N$.

E.1 The Fibonacci sequence

To explain how one can compute the structure factor of a quasicrystal and its periodic approximants, it is convenient to begin with a one dimensional example, the Fibonacci sequence. This 1D quasicrystal is an infinite sequence built of two kinds of tiles (line segments) called A and B. This quasicrystal can be lifted to a square grid in a 2D space by using the following rules: every A tile corresponds, in 2D, to a horizontal displacement $a\vec{u}_X$, and each B tile to a vertical displacement $a\vec{u}_Y$. This results in a broken path in 2D (see Fig.27) linking vertices that lie inside a stripe having a slope equal to λ_1^{-1} where $\lambda_1 = \frac{1+\sqrt{5}}{2}$ is the golden mean. Note that the same construction can be done for any other irrational slope like $\sqrt{3}/2$ (see section 5.3). The x axis is parallel to the strip, and represents the physical direction while the

y axis (not shown) is the perpendicular direction. The lengths of the A and B tiles are $x_A = a \cos \theta$ and $x_B = a \sin \theta$ respectively. The "selection strip" (so-called for evident reasons) has a width of $W = a(\cos \theta + \sin \theta)$ along the y -axis. The "composition space" for this and related binary structures is a line segment, where the two extremities represent periodic crystals: at one extremity is a tiling consisting only of A-tiles, and at the other only B-tiles. In the select-and-project method, these correspond to selection stripes with the angle θ equal to 0 and $\pi/2$, respectively (namely the stripes S_2 and S_1 in Fig.27). The periodic approximants of the Fibonacci sequence are obtained by stripes with the rational slopes F_{n-1}/F_n where the F_n are the Fibonacci numbers, obeying the recursion relation $F_n = F_{n-1} + F_{n-2}$ with $F_0 = F_1 = 1$. The sequence ABABABAB, for example, is a periodic approximant of slope $F_0/F_1 = 1$ ($\theta = \pi/4$), the next approximant is the sequence ABAABAABA... and has a selection stripe of slope $F_1/F_2 = 1/2$, and so on, the lengths of the approximants increasing with n , resulting in the Fibonacci sequence when n goes to infinity.

Thanks to this 2D representation of the quasicrystal it is simple to compute the Fourier transform (FT) of the Fibonacci sequence. We will assume the spatial distribution $\rho(x) = \sum_j \delta(x - x_n)$ where x_n is the coordinate of the n th site. In the 2D representation, the mass density can be expressed as a product, as follows

$$\rho(\vec{R}) = \rho_{sl}(\vec{R}) \chi(\vec{R})$$

$$\rho_{sl}(\vec{R}) = \sum_{m,n} \delta(\vec{R} - \vec{R}_{mn}) \quad (70)$$

where ρ_{sl} denotes the square lattice mass density, with $\vec{R}_{mn} = m\vec{u}_X + n\vec{u}_Y$ are the vertices. The function χ takes the value 1 if \vec{R} lies inside the strip, i.e if the projection $0 < \vec{R} \cdot \vec{u}_y < W$ and 0 otherwise. It follows from the relation 70 that the FT of the sequence is given by a convolution of the FTs of the square lattice, $\rho_{sl}(\vec{Q})$ – non-zero for $\vec{Q} = \vec{G}_{h,k} = \frac{2\pi}{a}(h\vec{u}_X + k\vec{u}_Y)$ – and that of the function χ , defined by

$$\chi(\vec{Q}) = \int d\vec{R} e^{i\vec{Q} \cdot \vec{R}}$$

$$\sim V \delta(q_x) \int_0^W dy e^{iq_y y} \chi(q_y) \quad (71)$$

In the second line above we have changed the integration variables in the rotated basis, where

$$q_x = \frac{2\pi}{a}(h \cos \theta + k \sin \theta)$$

$$q_y = \frac{2\pi}{a}(-h \sin \theta + k \cos \theta) \quad (72)$$

The resulting $S(q_x)$ has Bragg peaks along the q_x -axis at positions indexed by h, k . Their intensities are given by $|\chi(q_y)|^2 = \frac{4 \sin^2(q_y W/2)}{q_y^2}$. The projections of the 2D reciprocal lattice points gives rise to a dense set of Bragg peaks along the q_x axis. However the intensities for most of the peaks are negligibly small, and only a subset of the peaks corresponding to small q_y values are observable (see Fig.28). For approximants, the analysis proceeds along similar lines. The principal difference arises due to the fact that

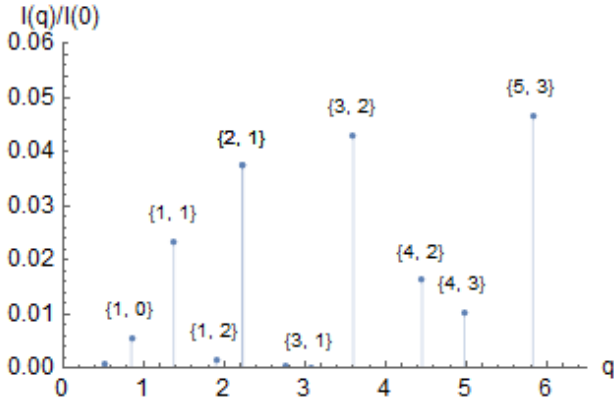


Fig. 28 Structure factor $S(q)$ plotted versus (physical space wave vector q (in units of 2π) for the perfect Fibonacci sequence. The indices above each peak indicate the corresponding 2D reciprocal lattice vector $\vec{G}_{h,k}$

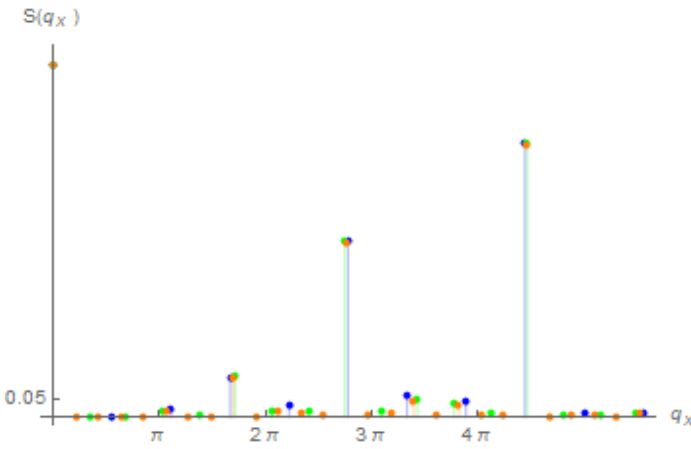


Fig. 29 Structure factors for three successive approximants of number of sites equal to 5 (blue), 8 (green) and 13 (orange).

the stripe has a rational slope. As a result, the Bragg peaks are spaced regularly with $\Delta q = 2\pi/L$, where L is the length of the approximant. Their intensities are given by the FT of the χ function defined with respect to the appropriate selection strip. The right-hand side of Fig.28 shows the structure factors of three approximant sequences to illustrate the manner in which the structure factor of approximants approach that of the infinite quasicrystal.

E.2 Square-triangle approximant phases

We can now extend these ideas to a perfect dodecagonal quasicrystal (ie, with no disorder) using the lift construction in the 4D superspace (see section A. In that case, the lifted vertices lie within an infinite stripe whose orientation is parallel to the physical axes. Their projections onto the perpendicular space P_\perp lie within a selection window W of finite extent and having a 12-fold symmetry (see Figure 14). As for the Fibonacci sequence, the mass density is a product of the 4D periodic lattice and a function χ . Thus the FT of the tiling is given by the convolution of two structure factors. The first is that of the 4D reciprocal lattice, (see section A.3), whose basis vectors project onto a star of 12 vectors

in the physical plane P . These are given by²⁸

$$G_n^* = \frac{2\pi}{a\sqrt{3}} \left(\cos \frac{(n-1)\pi}{6}, \sin \frac{(n-1)\pi}{6} \right) \quad (73)$$

where a is the edge length of the tiles. As was already noted in the real space description, only four of the twelve reciprocal lattice vectors G_n^* are rationally independent. They are labelled $(\mathbf{e}_1^*, \mathbf{e}_2^*, \mathbf{e}_3^*, \mathbf{e}_4^*)$ (see Figure 20 in section A.3). Thus, there are Bragg peaks at \vec{q}_\parallel positions which can be indexed by the integers h, k, l, m representing linear combinations of these four reciprocal lattice vectors. The intensities of each peak depends on these indices via the FT of the window W , and again, the observable peaks correspond to perpendicular space coordinates \vec{q}_\perp which are small ($aq_\perp \leq 1$).

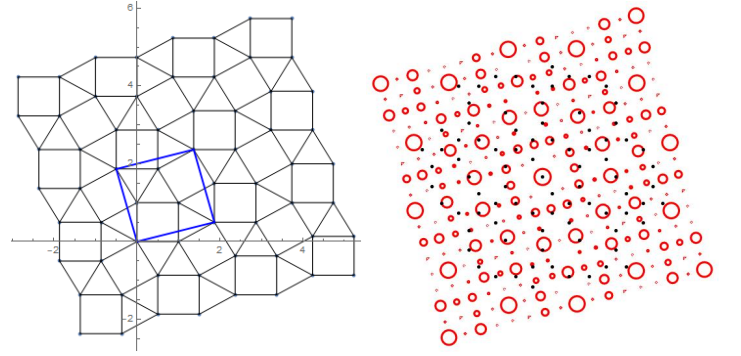


Fig. 30 (left) The sigma phase structure showing a unit cell outlined in blue. Its composition is given by $X = -0.268\dots$ and $Y = Z = 0$ with $\tau = 0.464\dots$ (right) Structure factor of the sigma phase in the (q_x, q_y) plane. Circles have radii corresponding to the peak intensity. Black dots indicate peak positions for the perfect quasicrystal showing the shifts due to finite global phason strain.

Turning next to the sigma phase shown in Fig. 30, the lift procedure yields a stripe which is inclined with respect to the plane P . This is encoded by the global phason strain B (see section 5.2). For this periodic approximant, the stripe has a rational direction in the 4D superspace. One can once again define a selection window by a region W in the plane perpendicular to the strip. As seen before for the approximants of the quasicrystal, the peaks in the reciprocal space \vec{q}_\parallel lie on a grid of spacing $2\pi/L$ where L is the period of the crystal. Fig.30 shows the structure factor – the radius of the red circles is proportional to the intensity of the peak. We note that these peaks are shifted with respect to the positions quasicrystal (shown by black dots) because the projection axes are slightly rotated with respect to the perfect QC.

A similar argument applies in the case of a bigger square approximant phase, of larger periodic length L based on repeating dodecagonal wheels as illustrated in Fig. 31. The structure factor of this phase is shown superimposed upon that of the sigma phase, showing the small shifts that occur when going from one approximant to the next. In the limit of the stripe becoming horizontal, one converges to the structure factor of the perfect quasicrystal.

Several comments are now in order. 1) in contrast to the Fibonacci sequence the window W has a fractal structure for the square triangle dodecagonal QC. As a result, Bragg peaks scale

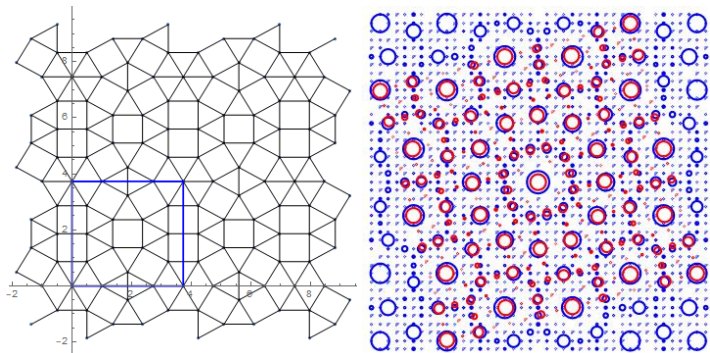


Fig. 31 (left) A periodic square approximant phase with the unit cell outlined in blue. Its composition is given by $X = 0.1436\dots$ and $Y = Z = 0$ with $\tau = 0.4897\dots$ (right) The structure factor shown by blue circles. At each peak position the circle size is proportional to the intensity.

as a fractional power in the system size rather than linearly. It would however be probably very difficult to experimentally measure this type of scaling. 2) The discussion given above can be extended to random tilings, for which the selection stripe has an irregular “wavy” form in 4D. The analysis in this case predicts a structure factor with broadened peaks of diminished intensity due to a disorder-induced Debye-Waller type factor, and in addition a diffuse background.²⁸